Cellular/Molecular

In Vivo Quantification of Myelin Changes in the Vertebrate Nervous System

Yanming Wang,[1] Chunying Wu,[1] Andrew V. Caprariello,[2] Eduardo Somoza,[1] Wenxia Zhu,[1] Changning Wang,[1] and Robert H. Miller[2]

[1]Division of Radiopharmaceutical Science, Case Center for Imaging Research, Department of Radiology, and [2]Department of Neurosciences, Case Western Reserve University, Cleveland, Ohio 44106

Destruction or changes associated with myelin membranes in the CNS play a key role in the pathogenesis of multiple sclerosis and other related neurodegenerative disorders. A long-standing goal has been to detect and quantify myelin content *in vivo*. For this reason, we have developed a myelin-imaging technique based on positron emission tomography (PET). PET is a quantitative imaging modality that has been widely used in clinical settings for direct assessment of biological processes at the molecular level. However, lack of myelin-imaging probes has hampered the use of PET for imaging of myelination in the CNS. Here, we report a myelin-imaging agent, termed Case Imaging Compound (CIC) that readily penetrates the blood–brain barrier and preferentially localizes to myelinated regions of the brain. After radiolabeling with positron-emitting carbon-11, [^{11}C]CIC–PET was conducted in longitudinal studies using a lysolethicin-induced rat model of focal demyelination and subsequent remyelination. Quantitative analysis showed that the retention of [^{11}C]CIC correlates with the level of demyelination/remyelination. These studies indicate that, for the first time, [^{11}C]CIC–PET can be used as an imaging marker of myelination, which has the potential to be translated into clinical studies in multiple sclerosis and other myelin-related diseases for early diagnosis, subtyping, and efficacy evaluation of therapeutic treatments aimed at myelin repair.

Introduction

Myelination is one of the most fundamental biological processes of vertebrate nervous system development (Sherman and Brophy, 2005). Myelin sheaths provide a unique structure in the nervous system that fosters rapid and efficient conduction of impulses along axons (Hildebrand et al., 1993). Abnormalities or changes in myelin occur in many acquired or inherited neurodegenerative diseases such as multiple sclerosis (MS), which affects an estimated 350,000 people in the US and 2 million people worldwide (Hauw et al., 1992). MS is characteristic of demyelination, resulting in axonal damage in the white matter. Recent efforts have been directed toward promoting endogenous myelin repair mechanisms and/or transplanting an exogenous source of myelinating cells to the demyelinated regions (Franklin and Hinks, 1999; Stangel and Hartung, 2002).

In parallel with these efforts, a major challenge has been to assess and quantify changes in myelin content *in vivo*. To date, magnetic resonance imaging (MRI) has been the primary tool for diagnosing and monitoring the progression of MS and related white matter diseases (Polman et al., 2005). However, MRI signals reflect a change of water content in tissues, which is a nonspecific measure of the overall changes in injury-induced macroscopic tissue structure, ranging from inflammation to axonal loss. As a result, MR imaging does not provide a direct measure of myelin content associated with demyelination and remyelination, and the use of MRI as a primary measure of disease activity was shown to be dissociated from clinical outcomes (Molyneux et al., 2001).

Positron emission tomography (PET), in contrast, is a functional imaging modality that has been widely used in clinical settings. Used in combination with a target-specific imaging agent, PET is capable of detection and quantification of biological processes at the molecular level. In MS, PET has been used to investigate the contribution of microglia activation to tissue destruction and disease progression, using a radioligand, termed [^{11}C]PK11195, that is specific for the peripheral benzodiazepine receptor (PBR) expressed by microglial cells (Cuzner, 1997; Wilms et al., 2003). [^{11}C]PK11195–PET imaging in MS patients demonstrated increased PBR expression in areas of focal pathology. However, PK11195–PET studies did not provide significant correlation with demyelination and are not a direct measure of myelin changes in the white matter. Lack of myelin-imaging agents has hindered the use of PET to directly assess myelination *in vivo*.

Recently, we have developed a family of bis-stilbene derivatives as myelin-imaging agents. We first reported a florescent myelin-imaging agent, termed BDB, that binds selectively to myelin membranes and is capable of detecting demyelinated lesions after intravenous injection (Wu et al., 2006). We also reported a carbon-11-labeled analog, termed [^{11}C]BMB, that has been used for PET myelin imaging in nonhuman primate (Stankoff et al.,

Received Aug. 26, 2008; revised Sept. 1, 2009; accepted Oct. 1, 2009.

We gratefully acknowledge the support from the National Multiple Sclerosis Society, the Myelin Repair Foundation, the Dana Foundation, and the National Institute of Neurodegenerative Disorders and Stroke (Grants R01 NS061837, NS054109).

Correspondence should be addressed to Dr. Yanming Wang, Division of Radiopharmaceutical Science, Case Center for Imaging Research, Department of Radiology, Bolwell S109, Case Western Reserve University, 11100 Euclid Avenue, Cleveland, OH 44106. E-mail: yanming.wang@case.edu.

DOI:10.1523/JNEUROSCI.4082-08.2009

 0270-6474/09/2914663-07$15.00/0

2006). The retention of [^{11}C]BMB was found in proportional to the level of myelinated fibers present in various brain regions.

Thus far, these myelin-imaging agents have been evaluated primarily through *in vitro* and *ex vivo* studies. While [^{11}C]BMB–PET has been conducted in normal nonhuman primates, no myelin-imaging studies have been conducted *in vivo* in animal models with demyelinating pathology. This is important as use of animal models of demyelination/remyelination will allow for validation of the imaging agents and evaluation of the imaging sensitivity. Therefore, we proceeded with *in vivo* PET studies in a rat model of focal demyelination/remyelination, using a carbon-11 labeled myelin imaging agent termed Case Imaging Compound or [^{11}C]CIC. CIC is another member of the bis-stilbene family we have developed as myelin-imaging agents. CIC shares the same pharmacophore as BDB and BMB. While these agents exhibit similar myelin-binding properties, we selected CIC for *in vivo* imaging studies in animal models of demyelination, and remyelination is due to the following considerations: Our previously reported BMB and BDB have moderate solubility, while CIC can be dissolved in many conventional solvents used for tissue staining and intravenous injections. In addition, the radiolabeling of BDB and BMB were not trivial, as the required precursors were not very stable and can be easily oxidized. As a result, BDB and BMB precursors are difficult to synthesize in a large quantity for storage and distribution. Compared with BDB and BMB, CIC possesses a structure that can be more readily radiolabeled than the other myelin-imaging agents we have reported. Thus, [^{11}C]CIC becomes the agent of choice for a series of animal studies. Here, we evaluated the pharmacokinetics and *in vivo* binding properties of [^{11}C]CIC. We also conducted the first longitudinal studies in a lysolethicin-treated rat model to monitor myelin changes *in vivo*. Such information provides further validation of [^{11}C]CIC–PET as a biomarker for myelination, which would represent a powerful tool for discovery and development of novel therapies aimed at prevention of demyelination and promotion of remyelination.

Materials and Methods

Radiosynthesis of [^{11}C]CIC. High specific radioactivity [^{11}C]methyl iodide was synthesized from [^{11}C]carbon dioxide using a custom-made one-pot reaction apparatus. Briefly, [^{11}C]carbon dioxide was produced by scanditronix MC17 cyclotron (10 min bombardment) and bubbled into a reaction device previously filled with $LiAlH_4$ in tetrahydrofurane (THF) solution (0.1 M, 1 ml) at room temperature. After THF was completely evaporated by argon gas, hydriodic acid (57%, 1 ml) was then added, and the device was heated to 120°C. [^{11}C]methyl iodide (3700 MBq) was distilled and trapped into a reaction vial containing the precursor BDB (2 mg), K_2CO_3 (10 mg), and dimethylformamide (DMF) (0.3 ml) at −70°C (dry ice) for 10 min. The reaction vial was then heated to 140°C for another 10 min and quenched with 10 ml of H_2O and cooled to room temperature. The resulting reaction mixture was loaded onto a Sep-Pak C-18 column and followed by washing with 10 ml of H_2O and rapid air bolus. The final product [^{11}C]CIC was eluted by 2 ml of ethanol and purified by HPLC [Phenomenex; C18, 250 × 10 mm, CH_3CN/H_2O = 80/20 (v/v), flow rate 3 ml/min]. The desired fractions were collected and evaporated to dryness under argon to give the final product [^{11}C]CIC (296 MBq). For injection, the residue was dissolved in 5% DMSO in saline and filtered through a 0.2 μm sterile membrane filter (Millex-GS Filter; Thermo Fisher Scientific) into a sterile vial. The total synthesis time was ~40 min (from [^{11}C]CH_3I); the radiolabeling yield was ~32% (decay corrected to $^{11}CH_3I$); and radiochemical purity was over 98% determined by radio-HPLC system. The chemical identity was verified by coinjection of the cold standard.

Measurement of octanol–water partition coefficient. Partition coefficient was measured by mixing the radioligands (radiochemical purity was >98%, ~500,000 cpm) with 1-octanol (3 g, 3.65 ml) and sodium phosphate buffer (PBS, 0.1 M, 3 g, pH 7.40) in a test tube. After consistent partitions of the coefficient values were obtained, the partition coefficient was determined by calculating the ratio of cpm/g of n-octanol to that of PBS. All assays were performed in triplicate.

Binding saturability assays. The saturation experiments were conducted using 12 × 75 mm borosilicate glass tubes. For each assay, an amount of 50 μl of the myelin suspension (2.5 μg of myelin membranes) were added to a series of solution each containing 10–120 μl of [^{3}H]-labeled myelin-binding agent. After diluted in PBS to a final volume of 500 μl, the assembled mixture was incubated at 37°C for 1 h. Triplets were used for each concentration. The bound and free radioligands were separated by rapid vacuum filtration through Whatman GF/B glass filter paper followed by 3 × 2 ml washes of PBS at room temperature. Filters containing the bound radioligand were placed in 6 ml of biodegradable counting mixture overnight, and the radioactivity was counted thereafter in the scintillation counter (Beckman) with 42% counting efficiency. Nonmyelin binding were determined by adding 50 μl of nonradiolabeled BMB (10 μM) in the same assay tubes each containing the same amount of radioligand and myelin protein. Triplets were also used for each concentration. Myelin binding was estimated as the difference between total and nonmyelin binding. The results were subjected to nonlinear regression analysis using Graph Pad Prism 4 software by which K_d and B_{max} will be calculated.

Ex vivo *characterization of CIC.* In this experiment, 10–100 mg/kg of cold CIC was injected intravenously through the tail vein of control. Animals were deeply anesthetized and perfused transcardially with 4% paraformaldehyde (PFA) in PBS 30 min and 18 h after injection. Brains were then removed from the calvarium, immersion postfixed in the same fixative solution, dehydrated in 30% sucrose, and embedded in freezing compound (O.C.T.; Miles Scientific) and cryostat sectioned at 20 μm and mounted on superfrost slides (Thermo Fisher Scientific). The pattern of myelination was assessed through Black–Gold labeling on adjacent sections according to the manufacturer's instructions. Sections were then examined with Olympus IX 51 microscope equipped with an Axiocam MRm digital camera and Axiovision 4.3 software.

Brain uptake studies. Mice (Swiss Webster, 22–24 g) received 2–22 MBq of high specific activity [^{11}C]CIC in 0.2 ml of buffered saline via the tail vein. The mice were killed by decapitation at various time intervals at 5, 30, and 60 min after injection. The brains were removed and collected, weighed, and counted. Radioactivity in tissue was assayed in an automated gamma counter, decay corrected to time of injection. The uptake of brain and blood were expressed in percentage injected dose (%ID) per gram organ. The percentage injected dose per gram organ of sample was calculated by comparing the sample counts with the count of the diluted initial dose. To remove the possible influence of brain blood volume, another three groups of mice (n = 3; 22–24 g) were perfused with saline followed by 4% PFA under anesthesia at 5, 30, and 60 min after injection of [^{11}C] CIC (2–20 MBq). The brains were then removed, collected, and assayed in an automated gamma counter, decay corrected to time of injection. The uptake of brain was expressed in %ID per gram organ.

Focal demyelination of adult rat brain. Sprague Dawley female rats, 6–8 weeks of age, were used for this study. Animal surgery and care was performed in accordance with the Institutional Animal Care and Use Committee of Case Western Reserve University. Animals were anesthetized using a mixture of ketamine hydrochloride (64.2 mg/kg), xylazine hydrochloride (12.9 mg/kg), and acepromazine (12.9 mg/kg) and positioned in a stereotaxic frame (Stoelting). A small incision was made in the scalp, and the corpus callosum was targeted using the following stereotaxic coordinates, relative to bregma: anterior–posterior, 0.0 mm; medial–lateral, 2.0; and dorsal–ventral, 3.4. A small hole was drilled in the skull, and a 26S gauge needle attached to a 10 μl Hamilton Syringe was lowered into the corpus callosum according to the dorsal–ventral coordinate. A microinjector pump (Stoelting) controlled the infusion of 6 μl of lysolethicin (lysophosphatidyl chorine) at a rate of 0.25 μl/min, after which the needle was left in place for 2 min to prevent liquid reflux out of the brain parenchyma. The incision was then closed using 5-0 Ethicon sutures, and the animals allowed to recover on a heating pad. MRI imaging and microPET imaging of demyelination of the rats were

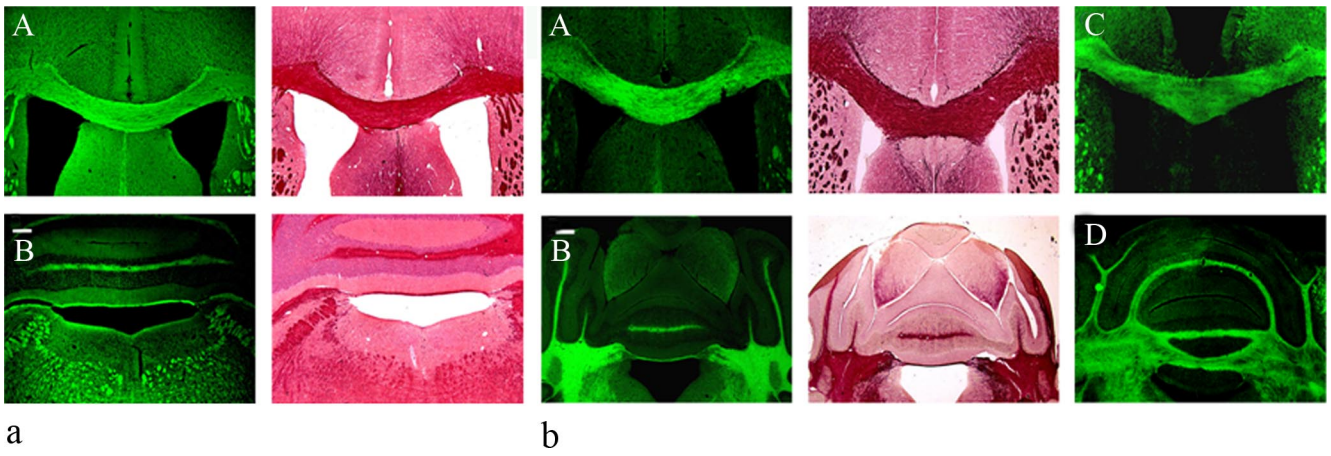

Figure 1. ***a***, Postmortem tissue staining in wild-type mouse brain demonstrates that in white matter regions such as corpus callosum (***A***) and cerebellum (***B***), CIC (green) labels myelin sheaths in a similar manner to standard myelin stains (pink, Black–Gold). Scale bar, 50 μm. ***b***, *In situ* CIC staining of myelin sheaths in the corpus callosum and cerebellum at 30 min (right panels; ***C***, ***D***) and 18 h (left panels; ***A***, ***B***) after administration of CIC through tail vein injection, which correlates with Black–Gold staining in adjacent sections (middle panels). Scale bar, 50 μm.

performed 5 d after surgery. The rats were kept alive. Another MRI imaging and microPET imaging of remyelination of the rats were conducted 1 month later.

MRI studies. All MRI imaging experiments were performed on a Bruker Biospec 7.0T/30 cm Magnetic Resonance Imaging and Spectroscopy scanner in the Case Center for Imaging Research at Case Western Reserve University (Bruker Biospin). The animal's head was then positioned in a 72 mm volume ID cylindrical transceiver coil. A RARE (rapid-acquisition relaxation-enhanced) acquisition (response time/echo time = 2000/40 ms, 4 echoes; field of view = 45 mm × 45 mm, matrix = 256 × 256) was used to acquire 15 contiguous 1 mm axial images of each animal's brain. The lesion area in each image was measured by selecting the conspicuous region of interest (ROI).

MicroPET studies. Animals were placed in a Concord R4 microPET scanner under anesthesia. After a 10 min transmission scan with a Co-57 source, 2 mCi/kg of radiolabeled agents were administered to each animal through a tail vein injection, which was immediately followed by dynamic acquisition for up to 90 min. List-mode emission data were analyzed as histograms with 12 × 5 s, 12 × 30 s, 5 × 60 s, and 17 × 300 s dynamic frames. A two-dimensional filtered back projection algorithm was used for image reconstruction with a 256 × 256 pixel resolution per transverse slice. A total of 63 transverse slices were reconstructed with a field of view covering the brain regions. Decay correction, attenuation correction, and scatter correction were all performed during the image histogram and reconstruction processes.

Coregistration of images and statistical analysis. Coregistration of MRI and PET images was conducted by using the MATLAB-based program COMKAT (Compartmental Model Kinetic Analysis Tool). The registration was conducted using a coronal view of the rats. After creating uniformed images from the PET and MRI images, VOI (volume of interest) and ROI were defined and used to measure the radioactivity concentration on one side of the corpus callosum (demyelinated) and its mirror counterpart on the other side of the corpus callosum (nondemyelinated). Multiple time activity curves were then obtained for statistical analysis. The radioactivity data were decay-corrected and normalized by the body weight of the rats and amount of [^{11}C]CIC injected. The resulting normalized time activity curves obtained from different data sets were averaged to obtain a representative normalized time activity curve for the experiments. A Student's *t* test was used to evaluate if there was any significant difference between the curves. A p value <0.05 was accepted as significant.

Tissue processing. After MRI and microPET studies, histological study was conducted. The animals were killed by way of transcardial perfusion of PBS followed by perfusion of 4% PFA under anesthesia. Brains were harvested and postfixed in 4% PFA for 2 h, after which they were cryoprotected in 30% sucrose overnight. Brain samples were then sectioned at 20 μm on a cryostat and mounted directly onto Superfrost Plus microscope slides. Using standard immuhistochemical techniques, slides were then treated with antibodies directed against Neurofilament (200 kDa; Millipore Bioscience Research Reagents) and GFAP (glial fibrillary acidic protein; Dako) to visualize axons and astrocytes, respectively. For Toluidine blue labeling, animals were fixed in electron microscopy fixative of 4% PFA and 2% glutaraldehyde. Vibratome sections (300 μm) were prepared through the area of interest and postfixed in 1% OSO_4. Tissue was dehydrated through graded ethanol and embedded in Epon 812. Transverse sections through the corpus callosum (1 μm thick) were labeled with Toludine blue.

Results

Lipophilicity

After synthesis and radiolabeling, the lipophilicity of [^{11}C]CIC was determined in terms of partition coefficients [octanol–water partition coefficient (logPoct)]. Using the conventional octanol–water partition method, we determined the logPoct value of [^{11}C]CIC as 2.36 ± 0.22 ($n = 3$). This value falls into the range for optimal brain permeability.

In vitro tissue staining of mice

CIC is a fluorescent compound. This allows us to evaluate its labeling properties based on fluorescent microscopy. We first examined the white matter binding property of CIC with fluorescent microscopy of mouse brain tissue sections. After the preparation of frozen sections of wild-type mice, fluorescent tissue staining was conducted with CIC and, for comparison, Black–Gold staining of myelin was performed on adjacent sections. Coronal sections were used so that both regions rich and poor in myelin could be easily compared. At a 10 μM concentration, CIC selectively labeled myelinated white matter regions such as the corpus callosum and cerebellum (Fig. 1*a*, left panel). The staining pattern using CIC was directly comparable with the pattern detected by Black–Gold staining. In sharp contrast, gray matter regions including those in the cerebellum and the frontal cortex showed little CIC staining. These studies demonstrate that CIC selectively labels white matter.

In vitro tissue staining of focal demyelination in rats

Based on the selective localization of CIC in myelinated white matter regions, we tested the possibility that CIC would be capable of detecting demyelinated lesions. We conducted CIC staining of tissue sections prepared from a rat model of focal demyelination. In this model, demyelination was induced by in-

jection of lysolethicin unilaterally into the corpus callosum to generate a focal demyelinated lesion. The presence of demyelinated foci was detected by fluorescent staining of serial sections with CIC (Fig. 2*A*). The same foci were confirmed by Black–Gold staining for myelin tracts in adjacent sections (Fig. 2*B*).

Our results demonstrate that injection of lysolethicin into rat corpus callosum results in a lesion due to focal myelin loss. To further characterize the selective loss of myelin with significant sparing of other cell types, we conducted additional immunohistochemical staining using antibodies directed against characteristic antigens expressed in both axons and astrocytes. As shown in Figure 3, other cell types such as axons and astrocytes are significantly spared, indicating the relative specificity of such an insult for myelin loss.

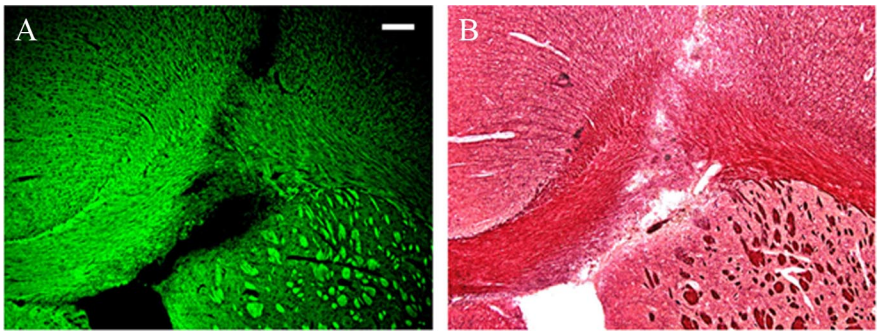

Figure 2. Postmortem tissue staining comparing CIC (***A***; green) to Black–Gold (***B***; pink) in an animal model of demyelination demonstrates the ability of CIC to detect myelin loss in rat corpus callosum. Scale bar, 50 μm.

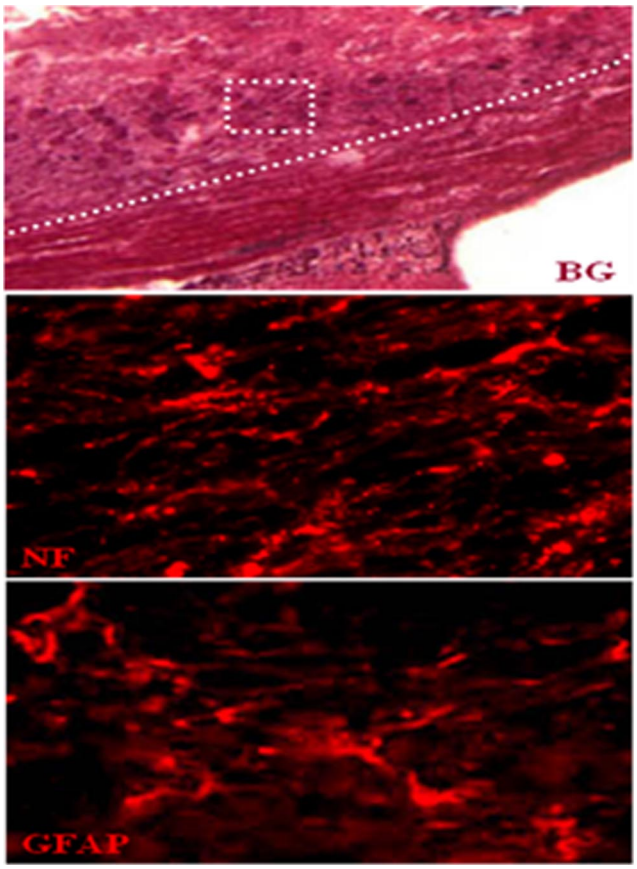

Figure 3. Lysolecithin injection into rat corpus callosum results in focal myelin loss [Black–Gold (BG), pink] but a relative sparing of axons [neurofilament (NF), red] and astrocytes (GFAP, red).

Saturation studies

To determine whether the binding of the bis-stilbene family molecules is saturable, we custom-labeled a previously reported CIC analog with tritium (^{3}H) termed [^{3}H]BMB and conducted saturation experiments using purified myelin membrane fractions. As shown in Figure 4, [^{3}H]BMB probe binds to myelin in a saturable manner, suggesting that there is a limited number of binding sites in myelin membranes. Scatchard analysis of the data demonstrates that the probe binds to a single population of binding sites with an equilibrium dissociation constant (K_d) of 1.098 nM and a maximal binding (B_{max}) of 17.61 pmol/mg protein. Since BMB and CIC are close analogs and exhibit similar binding properties, CIC also binds to myelin sheaths in a saturable manner with similar affinity.

Brain uptake studies in mice

CIC readily enters the mouse brain. After a single tail vein injection of [^{11}C]CIC, the radioactivity concentration of [^{11}C]CIC in the brain was determined at 5, 30, and 60 min after injection. Retention of [^{11}C]CIC in the brain was assayed with and without perfusion. Both assays show the same results, suggesting that the possible retention of [^{11}C]CIC in the brain blood volume is negligible. As shown in Figure 5, at 5 min after injection, the brain uptake reached 1.83 ± 0.22%ID/g. At 30 min, the brain concentration decreased to 2.30 ± 0.34%ID/g, and at 60 min, the brain concentration remained fairly steady (2.35 ± 0.30%ID/g, close to the 30 min value).

In situ tissue staining

After *in vitro* studies and brain uptake in rodents, we investigated the ability of CIC to stain myelinated white matter *in situ* in the mouse brain. A dose of 1.0 mg CIC (50 mg/kg) was injected via the tail vein into wild-type mice. At different time points (from 30 min to 18 h) after injection, mice were perfused with saline to clear the blood vessels in the brain, and the brains were then removed and sectioned. CIC staining of myelin was then directly examined under fluorescent microscopy. To demonstrate the time window of effective *in situ* myelin staining by CIC, brain tissue sections were prepared at 30 min and 18 h after CIC injection. The fluorescent images of corpus callosum and cerebellum are shown in Figure 1*b* in comparison with Black–Gold staining using adjacent sections. As shown in Figure 1*b* (right panels), CIC entered the brain and selectively labeled the corpus callosum and cerebellum as early as 30 min. The *in situ* staining can last as long as 18 h after injection (Fig. 1*b*, left panels). The patterns of CIC staining were consistent with subsequent Black–Gold staining in adjacent sections (Fig. 1*b*, middle panels), suggesting that CIC bound selectively *in situ* to white matter regions containing myelin fibers.

In vivo longitudinal microPET imaging studies

In this study, we used a rat model of focal, reversible CNS demyelination/remyelination for microPET imaging studies to take advantage of the relatively large size of the brain. The demyelinating agent lysolethicin was delivered to one hemisphere of the corpus callosum (Hall and Gregson, 1971). The axial views of

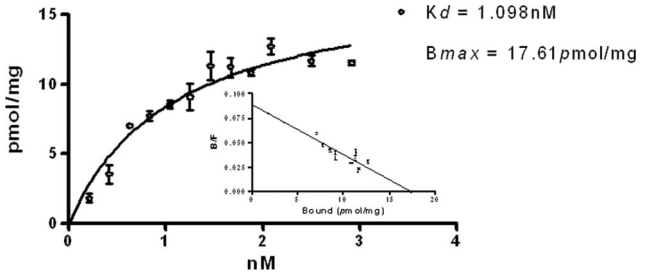

Figure 4. Representative saturation curve and Scatchard plot of the tritiated BMB binding to myelin fractions isolated from rat brain. Saturation studies were performed in a reaction mixture containing 50 μl of myelin fraction (2 μg protein in 1× PBS), 50 μl of the tritiated BMB (diluted in 1× PBS, 0.25–3.5 nM) in a final volume of 500 μl. Nonspecific binding was measured in the presence of excess (4000-fold) unlabeled probe (1 μM, diluted in 1% DMSO PBS) in the same assay tubes. The mixture was incubated at 37°C for 2 h, and the bound and the free radioactivity were separated by rapid vacuum filtration through Whatman GF/B filters using a Brandel M-24R cell harvester followed by 3 × 2 ml washes of PBS at room temperature. The results were analyzed with Graph Pad Prism 4, by which K_d and B_{max} values were calculated. Data are mean ± SD of three separate measurements done in triplicate.

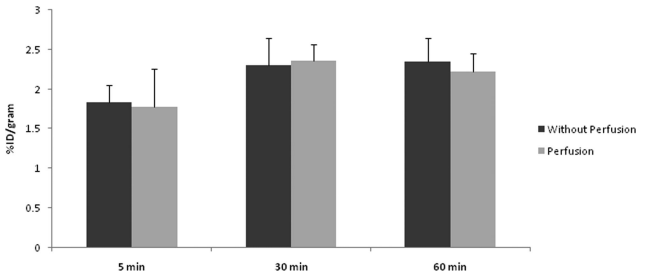

Figure 5. Kinetics of CIC accumulation in mice brain. [^{11}C]CIC was injected intravenously into normal control mice. At 5, 30, and 60 min after the injection, the mice were killed, and the brains were removed and weighed. Radioactivity in the brains was assayed in an automated gamma counter. The data were from three mice in each group and are showed as the mean ± SD of the whole-brain concentration relative to the injected dose (%ID/g).

both control and lysolethicin-treated rat brains are used to highlight the corpus callosum region. As shown in Figure 6, the anatomy of the rat brain and the focal lesion of demyelination induced in the corpus callosum region are illustrated by MRI images, which have been coregistered with microPET images. In comparison with the normal control rat, focal demyelination is readily detected 5 d after stereotaxic injection of lysolethicin to one hemisphere of corpus callosum, where the retention of [^{11}C]CIC is significantly decreased as indicated by the fused PET images. In addition, Figure 6 also shows that [^{11}C]CIC preferentially localizes in the myelin-rich white matter versus the myelin-deficient gray matter.

To assess whether [^{11}C]CIC allows for quantification of myelin loss, a longitudinal microPET imaging experiment after demyelination and subsequent remyelination in rat brain was performed. In the same rats, microPET and high resolution MRI imaging were conducted after demyelination and remyelination. The representative microPET images of normal, demyelinated, and remyelinated stages are shown in Figure 7. At the normal stage with intact myelination, [^{11}C]CIC uptake appears to be highest. After induction of demyelination, [^{11}C]CIC uptake was significantly decreased. After recovery, [^{11}C]CIC uptake was increased but still below the level observed in the normal stage.

For quantitative analysis, the microPET images were then registered with MR images for quantification of radioactivity concentrations. The left hemisphere of the corpus callosum, where demyelination was induced, was selected as the ROI for comparison. The average radioactivity concentrations during 0–60 min were determined. As shown in Figure 7, the uptake of [^{11}C]CIC in control rat brain was significantly higher than that in demyelinated rat brain, and as expected, the uptake of [^{11}C]CIC in demyelinated rat brain was significantly lower than that in remyelinated rat brain throughout the 60 min of microPET scan. In the corpus callosum, the average standardized uptake value (SUV) in the demyelinated region was 40 and 20% lower than those in the control myelinated region and remyelinated regions, respectively.

After PET imaging, we compared the ability of the CIC probe to detect formation of new myelin sheaths, a characteristic of the lysolethicin model of rat demyelination. To assess the level of remyelination, toluidine blue staining on sagittal sections of the corpus callosum were used immediately after PET imaging of remyelination. As shown in Figure 8, toluidine blue staining demonstrates disorganized but regenerated myelin after recovery compared with control sections taken from the contralateral hemisphere. We then compared these staining results to those obtained from [^{11}C]CIC–PET imaging. Interestingly, there were similar trends in the data: a decrease in the quantity of myelin at the peak of lysolethicin-mediated demyelination, followed by remyelination up to 6 weeks when the animal was killed. These results suggest that the [^{11}C]CIC–PET is a valid imaging marker for visualizing and quantifying myelin sheaths under both normal and pathophysiological conditions.

Discussion

Over the past years, we have developed a family of bis-stilbene derivatives as myelin-imaging agents. Previous studies focus primarily on the *in vitro* and *ex vivo* characterization of these myelin-imaging agents represented by BMB and BDB. So far, no *in vivo* studies have been conducted in animal models of demyelination and remyelination. In this study, we use one of the lead agents of the same class, termed CIC, for *in vivo* quantification of myelin changes in a rat model of focal demyelination/remyelination which can be conducted in a longitudinal manner.

We first evaluated the lipophilicity of CIC, which is an important factor in brain permeability. Previous study has shown that small-molecule compounds with a logPoct value ranging from 1.5 to 3.5 normally exhibit optimal brain uptake (Dishino et al., 1983). The logPoct of ^{11}C-labeled CIC was determined as 2.36 ± 0.22, falling into the range for optimal brain permeability. Indeed, [^{11}C]CIC can be administered to mice through tail vein injection with a brain uptake of 2.3%ID/g in average within 30–60 min, a level that is suitable for *in vivo* imaging studies (Fig. 5).

Fluorescent staining of mouse brain tissue sections indicated that CIC selectively stains white matter regions such as corpus callosum and cerebellum (Fig. 1*a*). After tail vein injection, CIC also readily penetrates the blood–brain barrier and selectively stains the same white matter regions *in situ* in a large time window (30 min to 18 h) (Fig. 1*b*). Since the images obtained at both early time point and later time point are very similar under the fluorescent microscope, we do not expect any significant difference in the labeling levels between 30 min and 18 h. Thus, the time course of the *in situ* staining was not quantitatively determined. The rationale for these studies was to demonstrate that CIC can readily enter the brain and be detected as early as 30 min and that it persists with the same distribution for at least 18 h. Importantly, CIC staining depends on the presence of myelin sheaths. In a rat model of focal demyelination as induced by lysolethicin, CIC is capable of detecting demyelinated lesions,

which is consistent with the conventional Black–Gold staining (Fig. 2). The immunohistochemical staining using antibodies directed against characteristic antigens expressed in both axons and astrocytes confirmed that the lysolethicin-induced lesions are caused by selective loss of myelin with significant sparing of other cell types (Fig. 3).

CIC represents a family of bis-stilbene derivatives that we have developed as myelin-imaging agents. The binding affinity of this class of compounds for myelin membranes was determined using a tritiated [^{3}H]BMB, an immediate analog of CIC. Due to the short half-life of carbon-11 ($t_{(1/2)}$ 20 min), we cannot use ^{11}C-labeled radioligands directly for binding assays and need to use tritiated radioligands instead so that radiolabeling does not result in any structural alteration. Because the half-life of H-3 is extremely long ($t_{(1/2)}$ ~4500 d), radiolabeling with H-3 needs to be contracted to a few designated laboratories where handling of large quantities of radioactive H-3 is licensed. Before our CIC studies, [^{3}H]BMB has already been made available to us through a contract with American Isotopes. Therefore, we used [^{3}H]BMB for the saturation studies to demonstrate the binding properties of this class of compounds. The binding of [^{3}H]BMB proves to be saturable (Fig. 4). Thus, it is reasonable to expect that CIC also binds to myelin in a saturable manner.

The reason we selected CIC for the *in vivo* imaging studies in the animal models is due to the fact that CIC can be more readily labeled with C-11. The labeling precursor of CIC is very stable and can be made in a large quantity for storage and distribution. It is also more soluble in conventional solvents for radiolabeling. In contrast, the labeling precursors of BMB and BDB are difficult to make and easily oxidized, making their storage and distribution very difficult. These studies suggest [^{11}C]CIC–PET is more practical for myelin imaging, which is why the reported studies were conducted with this agent.

After the above *in vitro* and *ex vivo* studies, we conducted microPET to directly quantify myelin changes *in vivo*. The goal was to assess and validate the myelin-imaging agent in animal models of demyelination and remyelination. Our microPET scanner (Concord R4) performs with ~2 × 2 × 2 mm image resolution (full-width at half-maximum), resulting in a volumetric resolution of ~8 mm^3 (Knoess et al., 2003). The size of de-

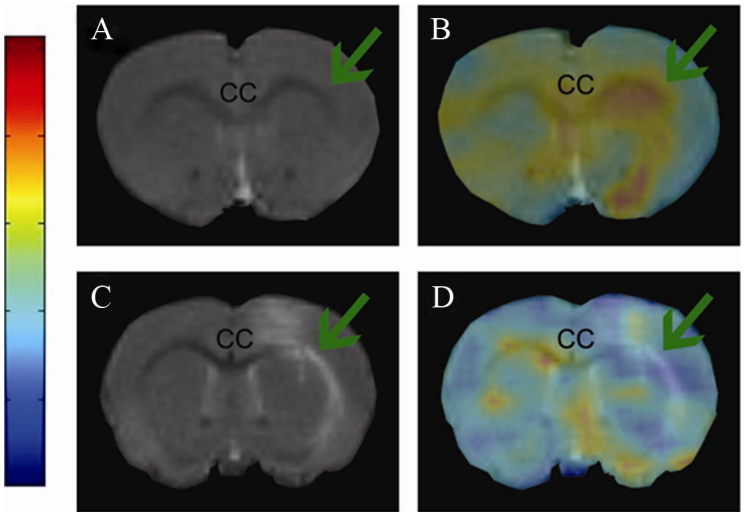

Figure 6. Axial views of corpus callosum of control and demyelinated rat model. Demyelination was induced via injection of lysolethicin directly into the right hemisphere of the corpus callosum as shown by the arrow. ***A***, MRI image of corpus callosum of control rat. ***B***, Fusion of MRI and PET images of corpus callosum of control rat. ***C***, MRI image of corpus callosum of demyelinated rat model. ***D***, Fusion of MRI and PET images of corpus callosum of demyelinated rat model.

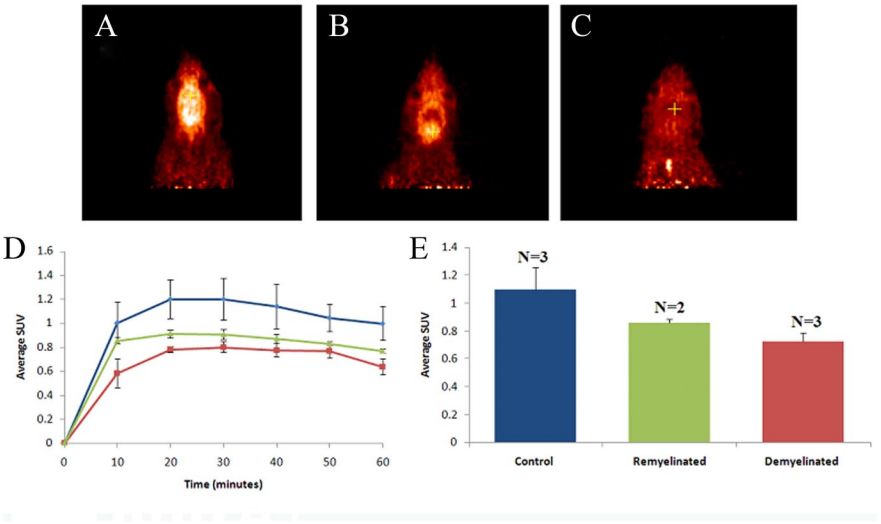

Figure 7. Images of microPET scans of rat models in order of increasing myelin content, control (***A***), remyelinated (***B***), demyelinated (***C***). ***D***, Average radioactivity concentration in terms of standardized uptake value *v* as a function of time in intact control region (blue) versus remyelinated region (green) versus demyelinated region (red) in right hemisphere of corpus callosum. ***E***, Average SUV of intact control (blue), remyelinated (green), and demyelinated regions (red) throughout the 60 min of scan with values of $p = 0.011$ for demyelinated versus remyelinated in corpus callosum. N, Number of mice averaged.

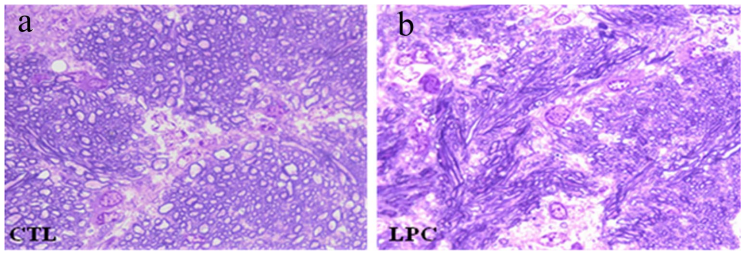

Figure 8. Toluidine blue staining of 1 μm lysolecithin-injected brain sections (***b***) demonstrate disorganized but regenerated myelin compared with control sections taken from the contralateral hemisphere (***a***).

myelinated lesions varies but can be induced to 5 mm in diameter on average. Therefore, microPET is capable of detecting and quantifying myelin changes in animal models. When demyelinated lesions are 2 mm or less, we would encounter the issue of resolution limitation of microPET. To address this issue, we first conducted high resolution of MR imaging. High resolution MR imaging with a typical in-plane resolution of 100 μm allows for accurate detection of lesions to define regions of interest. The microPET images were then registered with MR images so that radioactivity concentration could be quantified based on the regions of interest drawn on MR images (Fig. 6). Coregistration of MRI and microPET images is a widely used technique to overcome the resolution limitation of microPET and is routinely used in our brain imaging research.

Subsequently, we conducted longitudinal studies in the lysoethicin-treated rat model of focal demyelination and subsequent remyelination. As shown in Figure 7, [^{11}C]CIC–PET is capable to detect and quantify both demyelination and remyelination. The level of [^{11}C]CIC uptake was found to be in the same order of increasing myelin contents as presented in the demyelinated, remyelinated, and intact control stages, respectively. This is consistent with the pathological findings based on toluidine blue staining that shows disorganized but regenerated myelin after recovery (Fig. 8). As expected, the remyelination could only recover part of the myelin loss that is still below the level observed at the original control stage.

In summary, CIC has been developed as a myelin-imaging agent that readily penetrates the blood–brain barrier and binds to myelin membranes in the brain. Longitudinal [^{11}C]CIC–PET studies in lysolethicin-treated mouse model of focal demyelination shows that [^{11}C]CIC–PET can be used as an imaging marker to monitor time course of myelin changes *in vivo*.

References

Cuzner ML (1997) Microglia in health and disease. Biochem Soc Trans 25:671–673.

Dishino DD, Welch MJ, Kilbourn MR, Raichle ME (1983) Relationship between lipophilicity and brain extraction of C-11-labeled radiopharmaceuticals. J Nucl Med 24:1030–1038.

Franklin RJ, Hinks GL (1999) Understanding CNS remyelination: clues from developmental and regeneration biology. J Neurosci Res 58: 207–213.

Hall SM, Gregson NA (1971) The in vivo and ultrastructural effects of injection of lysophosphatidyl choline into myelinated peripheral nerve fibres of the adult mouse. J Cell Sci 9:769–789.

Hauw JJ, Delaère P, Seilhean D, Cornu P (1992) Morphology of demyelination in the human central nervous system. J Neuroimmunol 40:139–152.

Hildebrand C, Remahl S, Persson H, Bjartmar C (1993) Myelinated nerve fibres in the CNS. Prog Neurobiol 40:319–384.

Knoess C, Siegel S, Smith A, Newport D, Richerzhagen N, Winkeler A, Jacobs A, Goble RN, Graf R, Wienhard K, Heiss WD (2003) Performance evaluation of the microPET R4 PET scanner for rodents. Eur J Nucl Med Mol Imaging 30:737–747.

Molyneux PD, Barker GJ, Barkhof F, Beckmann K, Dahlke F, Filippi M, Ghazi M, Hahn D, MacManus D, Polman C, Pozzilli C, Kappos L, Thompson AJ, Wagner K, Yousry T, Miller DH, Miller DH (2001) Clinical-MRI correlations in a European trial of interferon beta-1b in secondary progressive MS. Neurology 57:2191–2197.

Polman CH, Reingold SC, Edan G, Filippi M, Hartung HP, Kappos L, Lublin FD, Metz LM, McFarland HF, O'Connor PW, Sandberg-Wollheim M, Thompson AJ, Weinshenker BG, Wolinsky JS (2005) Diagnostic criteria for multiple sclerosis: 2005 revisions to the "McDonald Criteria." Ann Neurol 58:840–846.

Sherman DL, Brophy PJ (2005) Mechanisms of axon ensheathment and myelin growth. Nat Rev Neurosci 6:683–690.

Stangel M, Hartung HP (2002) Remyelinating strategies for the treatment of multiple sclerosis. Prog Neurobiol 68:361–376.

Stankoff B, Wang Y, Bottlaender M, Aigrot MS, Dolle F, Wu C, Feinstein D, Huang GF, Semah F, Mathis CA, Klunk W, Gould RM, Lubetzki C, Zalc B (2006) Imaging of CNS myelin by positron-emission tomography. Proc Natl Acad Sci U S A 103:9304–9309.

Wilms H, Claasen J, Röhl C, Sievers J, Deuschl G, Lucius R (2003) Involvement of benzodiazepine receptors in neuroinflammatory and neurodegenerative diseases: evidence from activated microglial cells in vitro. Neurobiol Dis 14:417–424.

Wu C, Tian D, Feng Y, Polak P, Wei J, Sharp A, Stankoff B, Lubetzki C, Zalc B, Mufson EJ, Gould RM, Feinstein DL, Wang Y (2006) A novel fluorescent probe that is brain permeable and selectively binds to myelin. J Histochem Cytochem 54:997–1004.